The vanishing of strong turbulent fronts in bent pipes

Enrico Rinaldi[1], Jacopo Canton[1,†] and Philipp Schlatter[1]

[1]Linné FLOW Centre and Swedish e-Science Research Centre (SeRC), KTH Mechanics,
Royal Institute of Technology, SE-100 44, Stockholm, Sweden

Isolated patches of turbulence in transitional straight pipes are sustained by a strong instability at their upstream front, where the production of turbulent kinetic energy (TKE) is up to five times higher than in the core. Direct numerical simulations presented in this paper show no evidence of such strong fronts if the pipe is bent. We examine the temporal and spatial evolution of puffs and slugs in a toroidal pipe with pipe-to-torus diameter ratio $\delta = D/d = 0.01$ at several subcritical Reynolds numbers. Results show that the upstream overshoot of TKE production is at most one-and-a-half times the value in the core and that the average cross-flow fluctuations at the front are up to three times lower if compared to a straight pipe, while attaining similar values in the core. Localised turbulence can be sustained at smaller energies through a redistribution of turbulent fluctuations and vortical structures by the in-plane Dean motion of the mean flow. This asymmetry determines a strong localisation of TKE production near the outer bend, where linear and nonlinear mechanisms optimally amplify perturbations. We further observe a substantial reduction of the range of Reynolds numbers for long-lived intermittent turbulence, in agreement with experimental data from the literature. Moreover, no occurrence of nucleation of spots through splitting could be detected in the range of parameters considered. Based on the present results, we argue that this mechanism gradually becomes marginal as the curvature of the pipe increases and the transition scenario approaches a dynamical switch from subcritical to supercritical.

Key words: nonlinear instability, pipe flow boundary layer, transition to turbulence

1. Introduction

Over a century ago Osborne Reynolds observed that transition to turbulence in pipe flow is initiated by the appearance of localised travelling patches of chaotic motion (Reynolds 1883). He identified as the key parameter for the onset of turbulence the non-dimensional flow rate $Re = \bar{U}D/\nu$, later named the Reynolds number, where $\bar{U}$ is the mean flow speed, D is the pipe diameter and ν is the kinematic viscosity of the fluid. Successive experiments detailed this scenario and drew the distinction between turbulent spots that do not grow in size, puffs, and spots that expand in the

† Email address for correspondence: jcanton@mech.kth.se

surrounding laminar flow, slugs (see, e.g. Lindgren 1969, Wygnanski & Champagne 1973, Wygnanski, Sokolov & Friedman 1975; and the review by Mullin 2011).

Pipe flow presents the peculiarity of having a linearly stable laminar velocity profile (Meseguer & Trefethen 2003), i.e. all small perturbations decay and no critical Reynolds number can be defined using linear theory. However, experiments and simulations show that subcritical transition to turbulence can occur for $Re \gtrsim 1700$ if perturbations are sufficiently large. Only recently a statistical description of the intermittent flow in pipes has provided an accurate estimate of a critical Reynolds number, $Re \approx 2040$ (Avila *et al.* 2011). Below this threshold, the probability of a puff decaying outweighs the probability of a new puff being generated through a splitting mechanism. On the other hand, if the Reynolds number is higher than the threshold, the probability of splitting rapidly increases and puffs proliferate. Theoretical models have been proposed and quantitatively capture this subcritical transition scenario, which falls into the directed percolation universality class (Barkley 2011; Barkley *et al.* 2015; Shih, Hsieh & Goldenfeld 2015). For $Re \gtrsim 2300$ puffs turn into slugs, which rapidly fill the pipe thereby marking the onset of sustained space-filling turbulence. The reader is referred to the review by Barkley (2016) for further details.

The spatial structure of puffs and slugs has been the subject of several studies initiated by Wygnanski & Champagne (1973), Wygnanski *et al.* (1975) and followed by both experimental and numerical investigations (see e.g. Darbyshire & Mullin 1995; Nishi *et al.* 2008; and Duguet, Willis & Kerswell 2010; Song *et al.* 2017, respectively). Results show a high concentration of turbulent fluctuations at the strong upstream front and a gradual decrease at the weak downstream front. In fact, an instability is responsible for extracting energy from the upstream laminar flow and transferring it to the fluctuating field, while the downstream front corresponds to decaying turbulence. At sufficiently high Reynolds numbers, the weak downstream front turns into a strong front that feeds on the downstream laminar flow (Song *et al.* 2017). The core of the slugs was shown to have the same characteristics of a fully turbulent flow (see the previously referenced studies and also Cerbus *et al.* 2018).

Transition to turbulence in bent pipes has received less attention compared to straight pipes. For this flow case an additional governing parameter comes into play, namely the non-dimensional curvature $\delta = D/d$, with d indicating the coiling diameter. White (1929) was the first to observe that the flow in a bent pipe can be maintained in a laminar state for higher Reynolds numbers than in a straight pipe. More recent experiments by Sreenivasan & Strykowski (1983) reported relaminarisation of a turbulent flow entering a coiled pipe and provided Reynolds number ranges for subcritical transition to turbulence for low curvatures. However, this is not the only transition mechanism in bent pipes. Webster & Humphrey (1993, 1997), Kühnen *et al.* (2014) have reported supercritical transition from a steady to a periodic flow presenting a travelling wave for medium–high curvatures. Supercritical transition indicates a qualitative difference between straight and bent pipes, which are characterised by a modal instability for all curvatures different from zero (Canton, Schlatter & Örlü 2016). A unifying picture for transition in bent pipes was provided by Kühnen *et al.* (2015) who reported that subcritical transition dominates for $\delta \lesssim 0.028$, while above this value transition to turbulence occurs through a supercritical bifurcation cascade. Figure 2 reports the neutral curve for the flow in a torus (Canton *et al.* 2016) in the δ–Re plane, and experimental data indicating the onset of turbulence taken from the literature. Subcritical transition in bent pipes was described as being 'very similar as in straight pipes, where laminar and turbulent flows can coexist' (Kühnen *et al.* 2015). However, to the best of our knowledge,
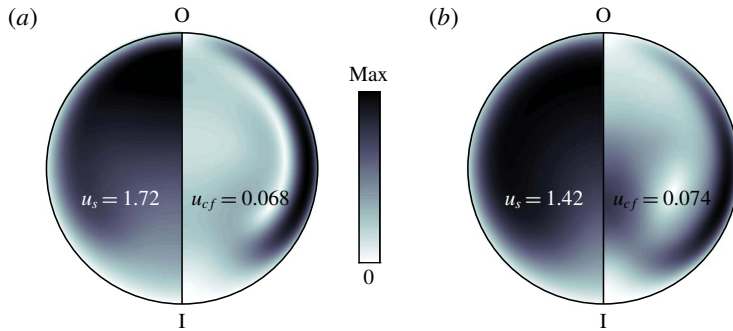
FIGURE 1. (Colour online) Cross-sectional velocity profiles of a laminar (*a*) and time-averaged turbulent (*b*) flow at $Re = 3000$ in a bent pipe with curvature $\delta = 0.01$. The inner and outer portions of the bend are indicated by I and O, respectively. The streamwise velocity u_s is displayed on the left half-section, while the cross-flow velocity u_{cf} is on the right half-section. The maximum values attained on the section are written in the figure.

an in-depth analysis of this regime is still missing. This is the focus of the present paper.

We perform direct numerical simulations (DNS) of the incompressible Navier–Stokes equations

$$\frac{\partial \boldsymbol{u}}{\partial t} + (\boldsymbol{u} \cdot \boldsymbol{\nabla})\boldsymbol{u} + \boldsymbol{\nabla}p - \frac{1}{Re}\nabla^2\boldsymbol{u} = \boldsymbol{f}, \tag{1.1}$$

$$\boldsymbol{\nabla} \cdot \boldsymbol{u} = 0, \tag{1.2}$$

where $\boldsymbol{u}$ is the velocity vector, p is the pressure, $Re = UD/\nu$ the Reynolds number (based on bulk velocity and pipe diameter) and $\boldsymbol{f}$ is a body force used to drive the flow in the toroidal geometry (a detailed discussion of $\boldsymbol{f}$ is given in Canton *et al.* 2016; Canton, Örlü & Schlatter 2017). Equations are discretised in space and integrated in time using the spectral element code NEK5000 (Fischer, Lottes & Kerkemeier 2008), which was previously validated on turbulent straight and bent pipes (El Khoury *et al.* 2013; Noorani, El Khoury & Schlatter 2013). The flow is kept at unitary bulk velocity as in Noorani *et al.* (2013), Canton *et al.* (2016). Exemplary laminar and turbulent velocity profiles in a bent pipe with $\delta = 0.01$ and $Re = 3000$ are displayed in figure 1. A detailed discussion of how the curvature affects the flow in the laminar regime is given by Canton *et al.* (2017).

In order to ensure that the nature of transition investigated here is subcritical, we choose $\delta = 0.01$. This curvature is sufficiently lower than the threshold for the onset of a supercritical bifurcation cascade ($\delta \approx 0.028$ according to Kühnen *et al.* 2015), while introducing a significant deviation of the laminar flow from that of a straight pipe (Canton *et al.* 2017). At $\delta = 0.01$, the laminar flow is linearly unstable for $Re > 4257$ (Canton *et al.* 2016). On the other hand, Kühnen *et al.* (2015) measured 50 % intermittency for $Re \approx 3000$ and numerical simulations show that the flow is in a sustained fully turbulent state above $Re = 3400$ (see Noorani *et al.* 2013; Noorani & Schlatter 2015). Figure 2 highlights the range of Reynolds numbers considered in the present study, $2900 \leqslant Re \leqslant 5000$, and gives an overview of our results in terms of turbulent structures. The large-scale evolution of puffs and slugs is studied in domains of length $L_s = 100D$ and $L_s = \pi d/3 \simeq 105D$ for straight and bent pipes
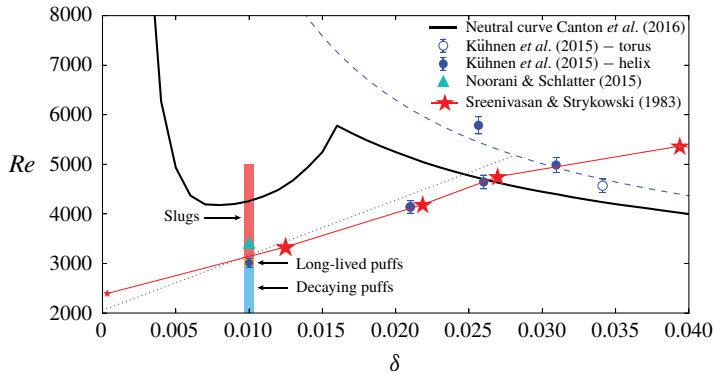
FIGURE 2. (Colour online) Stability map of the flow in a bent pipe. The continuous black line is the neutral curve calculated using linear theory (Canton *et al.* 2016). Red stars indicate the critical limit for transition as measured by Sreenivasan & Strykowski (1983). The triangle is a DNS of a fully turbulent flow by Noorani & Schlatter (2015). Circles are experiments by Kühnen *et al.* (2015) indicating 50 % intermittency (for $\delta \lesssim 0.028$) or the appearance of a periodic travelling wave. The blue lines are the interpolants by Kühnen *et al.* (2015) showing the onset of the subcritical transition (dotted) and of a supercritical bifurcation cascade (dashed). The coloured boxes indicate the flow regimes characterised in this paper: slugs ($Re > 3100$), long-lived puffs ($2950 < Re < 3100$) and decaying puffs ($Re < 2950$).

respectively, where the subscript s indicates the streamwise direction. Our spatial resolution satisfies typical DNS requirements for fully turbulent flows at Reynolds numbers slightly higher than the ones considered here.

The paper continues in § 2 with an analysis of the space–time dynamics of localised turbulent structures. Section 3 presents considerations on the budget of turbulent kinetic energy, and § 4 analyses the vortical structures embedded in puffs and slugs. Section 5 is dedicated to a discussion of the results.

2. Space–time dynamics of localised turbulence

We begin by examining how the space–time dynamics of localised turbulence is affected by the curvature. Figure 3 illustrates the main message of the paper by displaying the evolution of the cross-flow velocity fluctuations, q, for puffs (figure 3*a*) and slugs (figure 3*b*) in both straight and bent pipes. We use the scalar quantity q as an indicator of the level of turbulence in accordance with the literature regarding transitional flows in straight pipes (see, e.g. Barkley 2011) and adapt its definition to the case of bent pipes as

$$q(s, t) = \sqrt{\int_0^{2\pi} \int_0^R ((u_r - U_r)^2 + (u_\theta - U_\theta)^2) r \, dr \, d\theta}. \tag{2.1}$$

Here, s, r and θ indicate the streamwise, radial and azimuthal directions in toroidal coordinates. The instantaneous velocity components are $u_s = u_s(s, r, \theta, t)$, $u_r = u_r(s, r, \theta, t)$ and $u_\theta = u_\theta(s, r, \theta, t)$; capital letters denote the laminar flow at a given curvature and Reynolds number; $U_r = U_r(r, \theta; \delta, Re)$ and $U_\theta = U_\theta(r, \theta; \delta, Re)$ are zero in a straight pipe but not in a curved one, where Dean vortices (Dean 1927) constitute
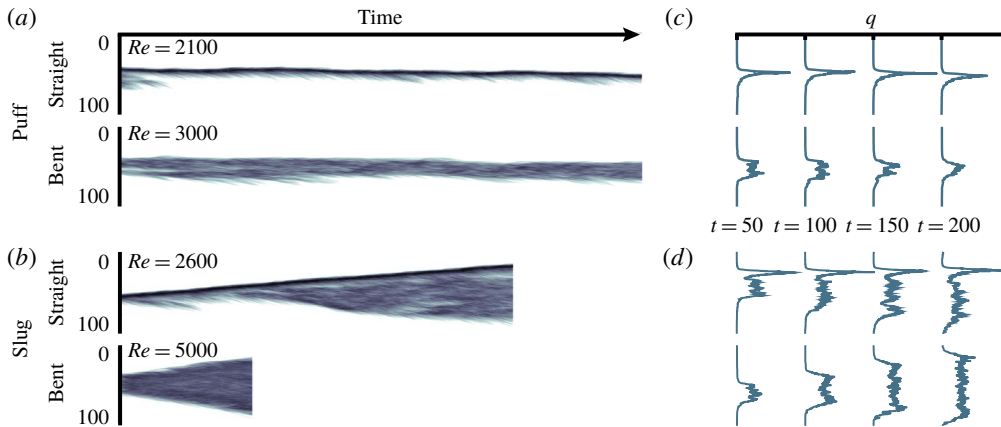
FIGURE 3. (Colour online) Space–time evolution of the cross-flow velocity fluctuations q, defined by (2.1), for exemplary puffs (*a*) and slugs (*b*) in straight and curved pipes. Colours represent $\log_{10} q$, white corresponds to laminar flow, dark colours to high fluctuations. Panels (*c*,*d*) report the spatial distribution of q sampled at four time instants. The (horizontal) scale used to indicate the magnitude of q is the same for the straight and curved pipes.

a secondary motion that can exhibit intensities comparable to that of the streamwise flow (Canton *et al.* 2017). We plot $q = q(s - u_f t, t)$, calculated in a frame of reference that moves with a constant streamwise velocity u_f, and use the same range of colour levels for straight and bent pipes to allow for a direct visual comparison. The reason for the different Reynolds numbers is that similar flow structures with similar characteristics, i.e. isolated puffs moving at approximately constant speed (figure 3*a*) and slugs expanding at a similar rate (figure 3*b*), are found at different Re in the two pipes.

A clear and distinctive feature differentiates puffs and slugs between the two pipes: the absence of a strong upstream front if the pipe is bent. Space–time diagrams show the well-known concentration of turbulent fluctuations, indicated by the dark tone of the colour, at the upstream front in straight pipes (Barkley 2011, 2016; Song *et al.* 2017). Conversely, the flow in a bent pipe shows no evidence of this strong front and is characterised by a somewhat uniform distribution of q. This is arguably the result of a gradual process triggered by the presence of a curvature, which leaves no trace of the strong upstream front for $\delta = 0.01$. A further peculiarity is that puffs extend over a streamwise length that is approximately twice the one reported in the absence of curvature. One-dimensional profiles of q, sampled at several subsequent times, are reported in figure 3(*c*,*d*), and facilitate the comparison between the straight and bent pipe flow cases. The overshoot of turbulent fluctuations is prominent if the pipe is straight and can reach values significantly higher than those downstream of the front, while in the curved pipe the upstream front has intensity comparable to that of the core of the structure.

The structure of puffs and slugs is quantitatively characterised by means of a projection of the flow trajectory on the u_s–q phase space (Song *et al.* 2017), with u_s now being the maximum streamwise velocity on the cross-section on which q is calculated. Figure 4 presents the data for a single realisation of a slug in a straight pipe at $Re = 2600$ and three slugs in a bent pipe at $Re = 3100$, 3300 and 5000.
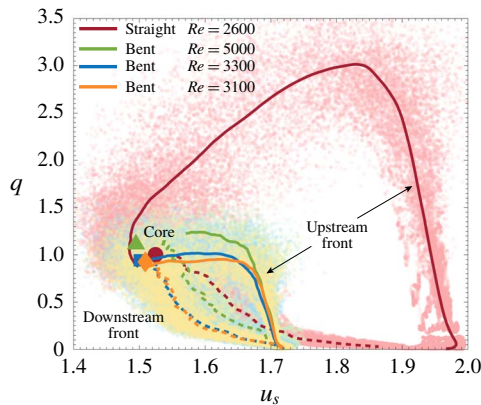
FIGURE 4. (Colour online) Trajectories of turbulent slugs in the u_s–q phase space for straight and curved pipes. The clouds indicate a subset of the instantaneous values. Lines indicate the average over time of values at the upstream front (solid) and at the downstream front (dashed). Large filled symbols are space–time averages in the core of the slug. Values of q are normalised by the average turbulent fluctuations in the core of the slug in the straight pipe at $Re = 2600$.

The loops for each flow case are obtained by time averaging u_s–q pairs over a length of 20 diameters across the upstream and the downstream fronts. Large filled symbols are space–time averages of the trajectory in the core. All values of q are normalised by the average turbulent fluctuations in the core of the slug in the straight pipe at $Re = 2600$. Moving in the direction of the flow, which corresponds to following loops in anti-clockwise direction starting from $q = 0$, the laminar velocity profile flattens, which is indicated by a decrease of u_s, and the turbulent fluctuations rapidly increase. The overshoot of q is clearly visible in the case of straight pipe, where maximum values can be over three times larger than in the core. On the other hand, if the pipe is bent, q settles to approximately the same value attained in the core in a nearly monotonic fashion.

The steep increase of q is a common feature of the upstream fronts in straight and bent pipes, and indicates that a similar mechanism of instability sustains the slug by extracting energy from the surrounding laminar flow. This is a key similarity that suggests that the analogy between transitional pipe flow and an excitable medium (Barkley 2012), such as a nerve axon, still holds in its essence if the pipe is bent. However, our results indicate a significant reduction of super-threshold perturbations at the upstream front as the curvature increases. This goes hand in hand with the emergence of strong Dean vortices that enhance the mixing and redistribution of turbulent fluctuations (the supplementary movie 1, available at https://doi.org/10.1017/jfm.2019.120, gives a graphical representation of the action of Dean vortices). As opposed to the upstream front, the downstream front corresponds to decaying turbulence, as in straight pipes.

The features of puffs and slugs discussed above are not affected by the choice of the parameter indicating the level of turbulence. The definition of q reduces the velocity field to a single scalar value by integrating over the cross-section of the pipe. This is a reasonable approximation in the case of a straight pipe, where the azimuthal direction is homogeneous. Nevertheless, q can still underestimate the level of turbulence in the presence of strong localisation in the radial direction. In the case of a bent pipe further
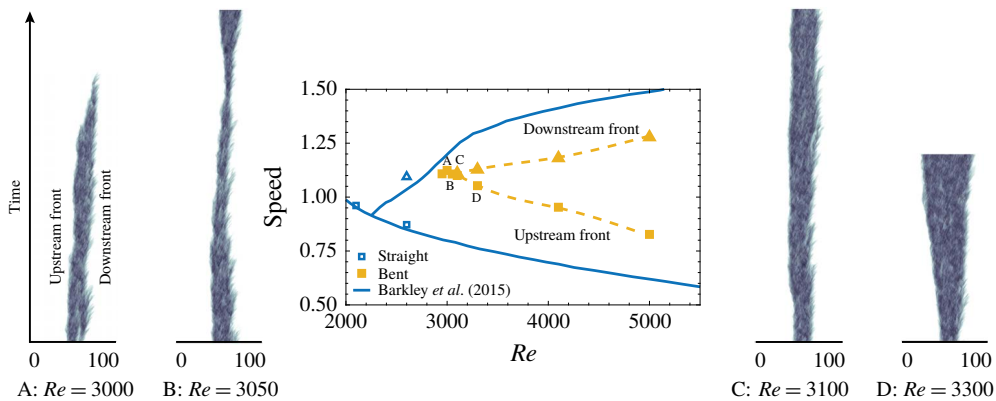
FIGURE 5. (Colour online) Front speed in straight (empty symbols) and bent pipes (filled symbols) as a function of the Reynolds number. Squares and triangles indicate the upstream and downstream fronts, respectively. At a given Re, a single entry in speed identifies a puff. The continuous line is the model from Barkley *et al.* (2015) for straight pipe. The dashed line guides the eye through the bent pipe data, but does not represent a model for the speed of the fronts. The lateral panels show the space–time diagrams corresponding to four selected cases. The time scale (vertical axis) is the same for all panels; the puff at $Re = 3000$ decays after $\tau \approx 700\,D/U$.

localisation can occur in the azimuthal direction, which is not homogeneous due to the curvature. We have verified that replacing (the average) q with its local maxima results in the same monotonic increase towards the core with no trace of overshoot.

Figure 5 presents a parametric study of the effect of the Reynolds number over the evolution of localised turbulence in the $\delta = 0.01$ bent pipe. The image includes space–time diagrams of q and an estimate of the velocity of the upstream and downstream fronts. The aim is to define an approximate lower bound on Re for long-lived localised turbulence in the form of puffs, and to pinpoint the onset of expanding turbulence. For our purpose, we set the definition of long-lived turbulence to a decaying time $\tau > 1000\,D/U$, which is shorter than the typical values used in straight pipes. As we will discuss in the following paragraphs, in bent pipes the separation in Reynolds number between the puff and slug regimes is much smaller than in straight pipes (Sreenivasan & Strykowski 1983). This indicates that for similar accuracy in Re shorter survival times for long-lived localised turbulent structures are sufficient.

Our results indicate that for $\delta = 0.01$ turbulence decays for Reynolds numbers below 2950. Isolated puffs seeded into a steady flow relaminarise, as do initially fully turbulent flows computed for higher Reynolds numbers, following a protocol analogous to Moxey & Barkley (2010). At $Re = 3000$ a single realisation of an isolated puff decays in approximately 700 advection time units (see point A in figure 5). On the other hand, a flow initialised with a fully turbulent field appears to persist as such. At $Re = 3050$ two simulations initialised with localised turbulence show no return to a laminar state. The first separation between the upstream and downstream fronts' speeds (approximately 1 %) occurs at $Re = 3100$ and marks the onset of the slug regime.

The limited number of realisations presented in this paper does not allow a precise computation of front speeds and decay times. Nonetheless, figure 5 provides an overview of the subcritical transition scenario in bent pipes and how it differs from

straight ones. We document an overall increase of the Reynolds numbers at which subcritical transition is triggered. The range of values at which long-lived localised turbulence persists is also significantly narrowed, reducing from $1900 < Re < 2300$ for a straight pipe to $2950 < Re < 3100$, above which puffs turn into slugs. The same behaviour was observed by Sreenivasan & Strykowski (1983) with experiments on helical pipes, and our numerical results are in good agreement with their data and with the Re value indicated by Kühnen *et al.* (2015) for 50 % intermittency.

The Reynolds number is not the only quantity to increase for bent pipes as compared to straight ones: the mean advection velocity of puffs and slugs is also larger. Puffs are faster than the bulk flow, while in a straight pipe they are slower, and the upstream front of slugs is slower than the mean flow only for $Re \gtrsim 3600$. Conversely, the expansion rate of slugs is reduced when compared to a straight pipe, indicating that these structures travel downstream more quickly but perturb a stationary point for a shorter time.

3. Turbulent kinetic energy budget

In order to get further insight into the structure of localised turbulence in bent pipes, figure 6 presents the budget of turbulent kinetic energy $k = 1/2 \, \overline{u'_i u'_i}$ calculated in the frame of reference co-moving with a slug and centred on the upstream front. The overline indicate time-averaged quantities and primes the fluctuation field $u'_i = u_i - \overline{u_i}$. Figure 6(*a*) presents the budget for a straight pipe at $Re = 2600$ and a comparison with data by Song *et al.* (2017). Figure 6(*b–d*) shows the present results in bent pipes for $Re = 3100$, 3300 and 5000. In the relative frame of reference the budget reads

$$\frac{\partial k}{\partial t} = P_k - \varepsilon_k - (\bar{u} - u_f)\hat{s} \cdot \nabla k - \nabla \cdot T_k = 0, \tag{3.1}$$

$$P_k = -\overline{u'_i u'_j} \frac{\partial \overline{u_i}}{\partial x_j}, \quad \varepsilon_k = \frac{2}{Re} \overline{s_{ij} s_{ij}}, \quad T_{k,i} = \frac{1}{2} \overline{u'_i u'_j u'_j} + \overline{u'_i p'} - \frac{2}{Re} \overline{u'_j s_{ij}}, \tag{3.2a-c}$$

where $s_{ij} = 1/2(\partial u'_i/\partial x_j + \partial u'_j/\partial x_i)$ indicates the shear rate, p is the pressure and $\hat{s}$ is the unit vector pointing in the streamwise direction. P_k, ε_k and $T_{k,i}$ are the production, dissipation and transport of turbulent kinetic energy, respectively. The terms in (3.1) are averaged over the pipe cross-section and normalised by the production rate in the core of each slug. As for q in the previous section, we have verified that using mean or local values does not affect the results.

The most striking difference between straight and bent pipes is the values of P_k and ε_k at the upstream front. While in a straight pipe the average production at the front is approximately five times higher than in the core, in a bent pipe it is only one-and-a-half times the value of the core. The second relevant difference is that in a straight pipe the peak of production precedes the peak of dissipation by approximately one pipe diameter, as can be seen in figure 6(*a*), while in a bent pipe they are almost at the same location (see (*b–d*)). Since for slugs in a bent pipe P_k and ε_k are in near equilibrium at each streamwise location, the rates of energy flux and convection provide a minor contribution to the budget.

One-dimensional budgets provide only partial information as bent pipes are not invariant to rotations on the section. As reported by Sreenivasan & Strykowski (1983) turbulent fluctuations in bent pipes appear first in the outer portion of the bend, while they pervade the whole cross-section only for higher Reynolds numbers. To complement figure 6, figure 7 presents the time-averaged distributions of production and dissipation over a cross-section of the pipe.
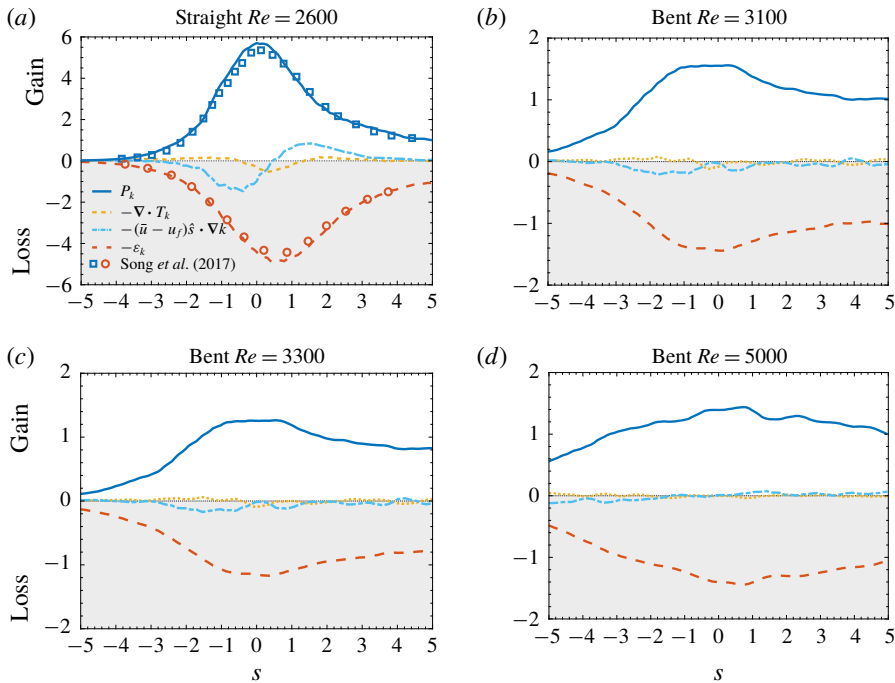
FIGURE 6. (Colour online) Turbulent kinetic energy budget integrated over the pipe cross-section in a straight pipe (*a*) and in a bent pipe for different Reynolds numbers (*b–d*). Panel (*a*) also reports the data by Song *et al.* (2017). The budget is calculated in a moving frame of reference centred at the upstream front of the slug. The terms of the budget are normalised by the value that P_k assumes in the core of the slug. Note the different scaling of the vertical axes.

The quantities in figure 7(*a–c*) are computed at the upstream front of slugs, which corresponds to $s = 0$ in figure 6. In a straight pipe P_k and ε_k are mainly concentrated in the near-wall region and in a ring around the centre of the pipe. Conversely, the budget in a bent pipe shows a high localisation towards the outside of the bend and lower peak values. This confirms that the vanishing of the strong upstream front is not an artefact of spatial averaging, but a specific feature pertaining to bent pipes. The cross-sectional localisation and lower local values of P_k and ε_k also suggest that an additional mechanism must come into play in sustaining turbulent patches. We argue that the secondary motion created by the Dean vortices is at the root of both these phenomena.

An insight in the spatial distribution of P_k at the front is given by considering perturbations whose integrated squared velocity is optimally amplified in the linear (small amplitude) and nonlinear (finite amplitude) regime, for a given time horizon. The structures corresponding to these optimal perturbations identify highly receptive regions of the flow where instabilities are likely to be triggered and lead to transition to turbulence.

In a straight pipe the linear optimal perturbation consists in a pair of large-scale low- and high-speed streaks, and corresponding counter-rotating vortices, which are located in the centre of the pipe. The nonlinear optimal perturbation, instead, is formed by streamwise and azimuthally localised streaks near the wall (see, e.g. Pringle & Kerswell 2010). The position of linear and nonlinear optimals corresponds
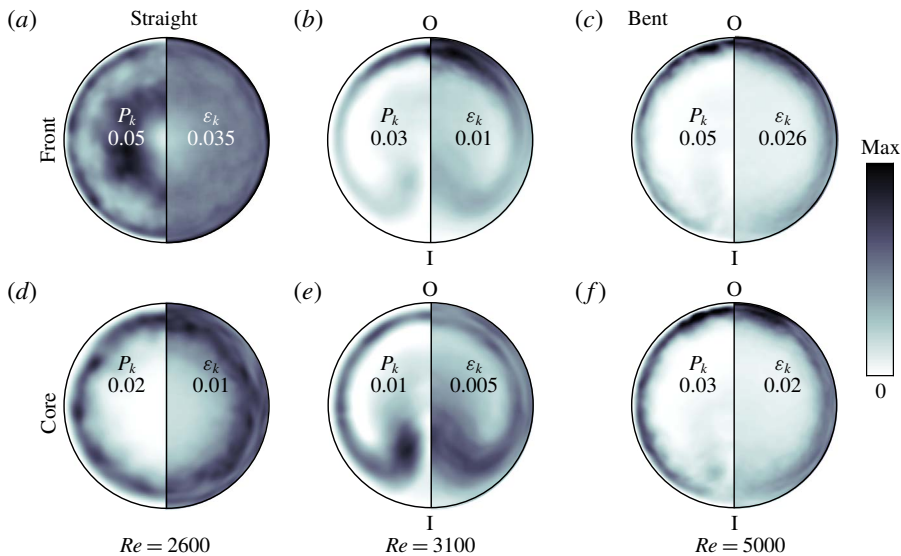
FIGURE 7. (Colour online) Turbulent kinetic energy production (left halves) and dissipation (right halves) at the front and core of slugs in straight and bent pipes. All quantities are averaged over time by tracking the slug, and over the cross-section taking into account the mirror symmetry of the torus, the axial invariance of the pipe has not been used in order not to alter the comparison. The text labels report the maxima of P_k and ε_k on each section (see also figure 6). The outer and inner portions of the bend are indicated by O and I, respectively.

to the peaks of turbulent kinetic energy production at the upstream front of puffs, thus suggesting a connection with the instability mechanisms that sustain the structure.

We have performed an analogous analysis for a bent pipe with $\delta = 0.01$ and present the results in figure 8. Linear optimals were calculated using the finite element code PASTA (Canton 2013; Canton *et al.* 2016). The figure shows the optimal perturbation calculated at $Re = 2870$, which is characterised by an energy gain of 106 by $t = 7.5$ with respect to the value at $t = 0$. The spatial distribution of the initial velocity field shows a strong cross-sectional localisation near the outer portion of the bend. In this region the streamwise velocity of the laminar base flow as well as its wall-normal derivative are largest, suggesting a large potential for extracting kinetic energy from the steady flow and converting it into the fluctuating field. The streamwise streaks are quickly amplified through the lift-up induced by the counter-rotating vortices and drift to the sides of the section as a consequence of the secondary motion induced by the Dean vortices, dissipating as they move away from the outer portion of the bend, and eventually disappearing entirely by the time they reach the inner bend.

Nonlinear optimal perturbations were calculated with NEK5000 using a gradient-based optimisation algorithm that relies on integrating backward in time the adjoint equations to compute the gradient (Pringle & Kerswell 2010). A checkpointing and revolve strategy was adopted in order to limit the memory requirements (Schanen *et al.* 2016). The initial condition is updated at each step of the optimisation using the gradient rotation algorithm (Foures, Caulfield & Schmid 2013). The nonlinear optimal perturbation at $Re = 3000$ with initial energy constrained to $E_0 = 4 \times 10^{-5} U^2$ (integrated over the volume) is shown in the figure. The length of the domain
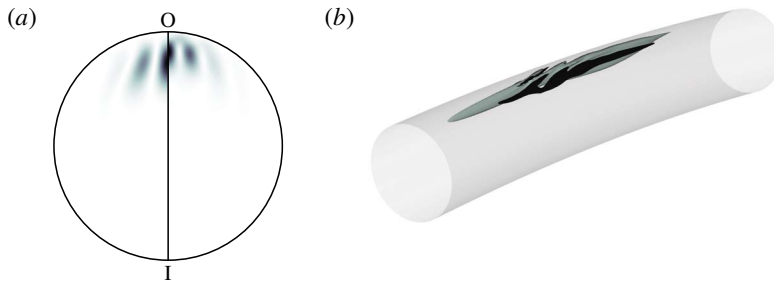
FIGURE 8. (Colour online) Optimal perturbations in a bent pipe. (*a*) Linear optimal initial condition: the left and right halves of the pipe section depict $E_{sw} = u_s^2/2$ and $E_{cf} = (u_r^2 + u_\theta^2)/2$, respectively. (*b*) Nonlinear optimal initial condition: contours of the streamwise velocity ($-3.5 \times 10^{-3} U$ and $2.5 \times 10^{-3} U$).

is $L_s = 2\pi D$. The optimisation was performed over a maximum integration time $T = 60D/U$, at which the energy gain of the converged optimal is 1074. Similarly to the linear optimal, the streaky velocity perturbations are localised near the outer bend. They undergo secondary instabilities leading to the transient appearance of hairpin vortical structures and are also subjected to the drift induced by the Dean vortices. Despite the significant energy amplification of the reported nonlinear optimal perturbation, its evolution beyond the optimisation time $T = 60D/U$ is marked by a decay and an eventual return of the flow to a laminar state. We have not searched for a minimal seed of turbulence, which implies a search over both E_0 and T parameter spaces and goes beyond the scope of the discussion of optimal perturbations within the present paper.

From the results presented it appears that the high receptivity of the region near the outer portion of the bend, where the recirculating mean flow impinges on the wall of the pipe, plays a primary role in feeding the upstream front of the puff and keeping it alive, as suggested by the location of the peak of P_k. Turbulent fluctuations generated here are then transported along the walls of the pipe and lifted up towards the inner section.

Figure 7(*d–f*) presents the distribution of production and dissipation at the core of the slugs. In a straight pipe the ring of high P_k, which was observed at the front, disappears. Production and dissipation are localised in the near-wall region and are the same as in a fully turbulent pipe flow. For high Reynolds numbers, when slugs expand rapidly, the spatial distributions of P_k and ε_k in bent pipes are qualitatively unchanged between the front and the core, as can be seen in figure 7(*c,f*). At intermediate Reynolds numbers, instead, the cores are qualitatively different. The peaks of P_k and ε_k are localised in two lobes in the proximity of the inner bend of the pipe, near the symmetry axis, as can be seen in figure 7(*b,e*) for $Re = 3100$. The same behaviour is observed for $Re = 3300$ (not shown in the figure). These lobes are likely connected with a low frequency, highly energetic mode responsible for the so-called sublaminar drag in the range $2900 \lesssim Re \lesssim 4000$ (Noorani & Schlatter 2015).

4. Vortical structures at the front

We conclude our analysis by discussing the dynamics of vortical structures at the upstream front of slugs. Figure 9 reports instantaneous fields of vortices visualised

(*a*)

Straight $Re = 2600$

(*b*)

Bent $Re = 3300$ (calm)

(*c*)

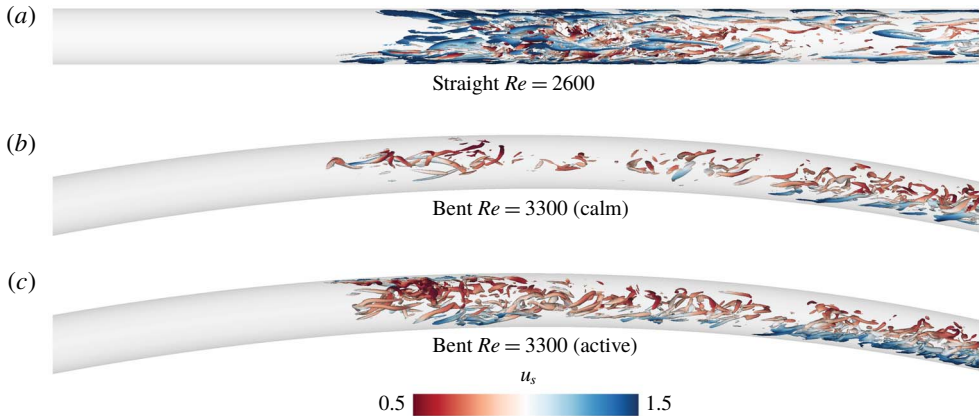Bent $Re = 3300$ (active)

u_s

0.5 ▮▮▮▮▮ 1.5

FIGURE 9. (Colour online) Snapshots of the flow at the upstream front of a slug. The figure depicts iso-contours of negative λ_2 coloured by streamwise velocity magnitude. The slug in the bent pipe is represented in both its 'calm' and 'active' phases. See also the supplementary movies 1–4.

using the λ_2 criterion (Jeong & Hussain 1995) for both straight and bent pipes. This method identifies the vortex core using the second eigenvalue of the symmetric tensor $\boldsymbol{S}^2 + \boldsymbol{\Omega}^2$, with $\boldsymbol{S}$ and $\boldsymbol{\Omega}$ indicating the symmetric and antisymmetric parts of the velocity gradient tensor.

The flow in a straight pipe shows a high concentration of vortices at the upstream front, distributed in the typical conical shape going from the near-wall region towards the centre (figure 9*a*). These vortices form a relatively sharp boundary with the laminar flow upstream of the front and are generated at an approximately constant rate, as can be seen in the supplementary movie 2. Their concentration in the centre of the pipe reduces downstream of the front and is limited to the near-wall region, consistently with the distribution of P_k discussed in §3.

If the pipe is bent, the upstream front gradually emerges from the laminar flow and is considerably less densely populated by vortical structures. The generation of new vortices is modulated in time and is organised over the succession of 'active' and 'calm' phases, see figure 9(*b,c*) and supplementary movies 3–5. This is particularly evident for moderately expanding slugs. During the active phase new vortices are generated at the outer bend, where P_k is maximum and perturbations are amplified, as discussed in §3. During the calm phase vortical structures are generated at a lower rate near the centre of the pipe. The alternation of calm and active phases is illustrated in figure 10, which reports the time history of the friction Reynolds number and of the total perturbation kinetic energy. The former is defined as $Re_\tau = (Re/\nu)\sqrt{(R/2\rho)(\mathrm{d}p/\mathrm{d}s)}$, and is computed using the mean pressure gradient calculated over the entire domain. The latter reads $E_{tot} = (1/2)\int_{Vol}\sum\Delta u_i^2\,\mathrm{d}V$, with $\Delta u_i = u_i - U_i$, and is calculated on a 20-diameter long moving frame of reference centred on the upstream front of the slug. The signal of Re_τ shows a decreasing trend that is consistent with the fact that a fully turbulent flow at $Re = 3300$ is characterised by sublaminar drag (see Cioncolini & Santini 2006; Noorani & Schlatter 2015). Active and calm phases appear as local oscillations on top of this trend. In particular, active phases correspond to a local plateau and subsequent decrease in the profile of Re_τ, and are connected by calm phases where Re_τ reaches a local minimum before
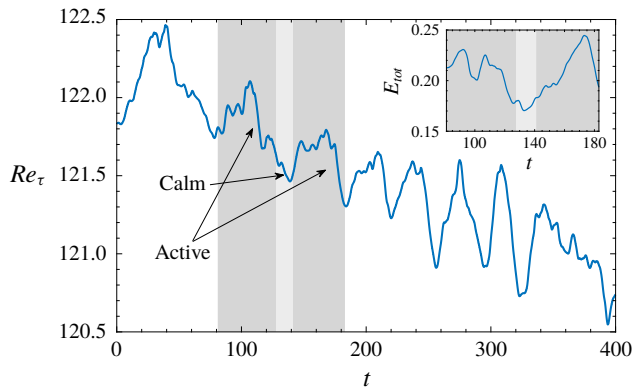
FIGURE 10. (Colour online) Time history of the friction Reynolds number (Re_τ) calculated over the whole computational domain, and of the perturbation kinetic energy (E_{tot}) calculated on a subdomain co-moving with the upstream front of the slug at $Re = 3300$. Dark and light shaded areas highlight examples of active and calm phases at the front.

starting to rise again. Active phases typically last for a time $t = O(40\,D/U)$, while calm phases are shorter, $t = O(20\,D/U)$. Since Re_τ is based on an integral quantity calculated over the whole computational domain, which is filled by the turbulent slug as time advances, the effect of the dynamics at the front is gradually less visible. The perturbation kinetic energy calculated across the slug front shows that active phases consistently correspond to high values of E_{tot}.

In addition to the spatial localisation and lower values of P_k discussed in §3, the temporal modulation also contributes to weaker upstream fronts if compared to straight pipes. To the best of our knowledge, this is the first time this phenomenon is documented on the fronts of expanding turbulence in pipe flows.

The curvature also influences the transport of vortices inside the slug. This can be clearly seen in the supplementary movie 1, which presents a comparison between a straight and a bent pipe. The video shows vortical structures in a one diameter long section as seen from inside the pipe while following the upstream front. While in the straight pipe the vortices move chaotically, in the bent pipe they are clearly transported in a coherent circulatory motion dictated by the Dean vortices. This visually shows how a localised production of vortices is sufficient to sustain the extended structure of a slug.

5. Summary and conclusions

We have studied the dynamics of localised turbulent structures in a bent pipe with curvature 0.01. The analysis was performed by means of direct numerical simulations for Reynolds numbers between 2900 and 5000. Our results show that subcritical transition to turbulence occurs over $2950 \lesssim Re \lesssim 3100$, where laminar and turbulent flow coexist in an intermittent fashion. The indicated range is significantly narrower than the one documented for a straight pipe, which is in good agreement with the literature on the subject (see, e.g. Sreenivasan & Strykowski 1983; Kühnen *et al.* 2015).

Localised turbulent structures in bent pipes bear qualitative similarities to those in straight pipes in that they appear in the form of puffs and slugs that are sustained

by an instability at their upstream front. However, the most striking difference is that the strong upstream front vanishes if the pipe is bent. We report velocity fluctuations that are three times smaller than the ones observed in straight pipes. Furthermore, the turbulent kinetic energy budget shows that production at the front is at most one-and-a-half times the one in the core of the slug, while in straight pipes it is up to five times larger than in the core. Production and dissipation are strongly localised towards the outer bend, in a region that is highly receptive to flow perturbations. We argue that the emergence of a strong secondary flow (Dean 1927) is responsible for the localisation and is crucial for the effective mixing of vortical structures. A further peculiarity encountered in bent pipes is that the generation of vortices at the front occurs through a succession of active (longer) and calm (shorter) phases, which contribute to the overall small values of production and dissipation. This is to the best of our knowledge the first time that such temporal modulation of the upstream front is reported in pipe flows.

The final difference between bent and straight pipes is the apparent absence of puff splitting when the pipe is bent, at least for the choice of parameters investigated here. Since the genesis of a child puff from a mother puff is a statistical (non-deterministic) phenomenon, we cannot completely exclude it based on our limited number of simulations. A thorough, possibly experimental, investigation focused on this phenomenon should be performed to verify our claim. We conjecture that the absence of puff splitting is connected to the weakness and cross-sectional localisation of the upstream fronts. Turbulent structures protruding from the downstream front of the mother puff into the surrounding laminar flow (Avila *et al.* 2011) have a low probability of entering the small region of high amplification located near the outer wall. Moreover, due to the secondary motion, the few vortical structures that visit this region do not linger for long enough to sustain a new puff after the separation between mother and daughter (Shimizu *et al.* 2014).

Acknowledgements

Supplementary movies

Supplementary movies are available at https://doi.org/10.1017/jfm.2019.120.

REFERENCES

AVILA, K., MOXEY, D., DE LOZAR, A., AVILA, M., BARKLEY, D. & HOF, B. 2011 The onset of turbulence in pipe flow. *Science* **333** (6039), 192–196.

BARKLEY, D. 2011 Simplifying the complexity of pipe flow. *Phys. Rev.* E **84** (1), 016309.

BARKLEY, D. 2012 Pipe flow as an excitable medium. *Rev. Cub. Fis.* **29** (1E), 27–30.

BARKLEY, D. 2016 Theoretical perspective on the route to turbulence in a pipe. *J. Fluid Mech.* **803**, P1.

BARKLEY, D., SONG, B., MUKUND, V., LEMOULT, G., AVILA, M. & HOF, B. 2015 The rise of fully turbulent flow. *Nature* **526** (7574), 550–553.

CANTON, J. 2013 Global linear stability of axisymmetric coaxial jets. Master's thesis, Politecnico di Milano, Italy.

CANTON, J., ÖRLÜ, R. & SCHLATTER, P. 2017 Characterisation of the steady, laminar incompressible flow in toroidal pipes covering the entire curvature range. *Intl J. Heat Fluid Flow* **66**, 95–107.

CANTON, J., SCHLATTER, P. & ÖRLÜ, R. 2016 Modal instability of the flow in a toroidal pipe. *J. Fluid Mech.* **792**, 894–909.

CERBUS, R. T., LIU, C.-C., GIOIA, G. & CHAKRABORTY, P. 2018 Laws of resistance in transitional pipe flows. *Phys. Rev. Lett.* **120**, 054502.

CIONCOLINI, A. & SANTINI, L. 2006 An experimental investigation regarding the laminar to turbulent flow transition in helically coiled pipes. *Exp. Therm. Fluid Sci.* **30** (4), 367–380.

DARBYSHIRE, A. G. & MULLIN, T. 1995 Transition to turbulence in constant-mass-flux pipe flow. *J. Fluid Mech.* **289**, 83–114.

DEAN, W. R. 1927 Note on the motion of fluid in a curved pipe. *Lond. Edin. Dublin Phil. Mag. J. Sci.* **4**, 208–223.

DUGUET, Y., WILLIS, A. P. & KERSWELL, R. R. 2010 Slug genesis in cylindrical pipe flow. *J. Fluid Mech.* **663**, 180–208.

EL KHOURY, G. K., SCHLATTER, P., NOORANI, A., FISCHER, P. F., BRETHOUWER, G. & JOHANSSON, A. V. 2013 Direct numerical simulation of turbulent pipe flow at moderately high Reynolds numbers. *Flow Turbul. Combust.* **91** (3), 475–495.

FISCHER, P. F., LOTTES, J. W. & KERKEMEIER, S. G. 2008 Nek5000 web page http://nek5000.mcs.anl.gov.

FOURES, D. P. G, CAULFIELD, C. P. & SCHMID, P. J. 2013 Localization of flow sstructure using ∞-norm optimization. *J. Fluid Mech.* **729**, 672–701.

JEONG, J. & HUSSAIN, F. 1995 On the identification of a vortex. *J. Fluid Mech.* **285**, 69–94.

KÜHNEN, J., BRAUNSHIER, P., SCHWEGEL, M., KUHLMANN, H. C. & HOF, B. 2015 Subcritical versus supercritical transition to turbulence in curved pipes. *J. Fluid Mech.* **770**, R3.

KÜHNEN, J., HOLZNER, M., HOF, B. & KUHLMANN, H. C. 2014 Experimental investigation of transitional flow in a toroidal pipe. *J. Fluid Mech.* **738**, 463–491.

LINDGREN, E. R. 1969 Propagation velocity of turbulent slugs and streaks in transition pipe flow. *Phys. Fluids* **12** (2), 418–425.

MESEGUER, Á. & TREFETHEN, L. N. 2003 Linearized pipe flow to Reynolds number 10^7. *J. Comput. Phys.* **186** (1), 178–197.

MOXEY, D. & BARKLEY, D. 2010 Distinct large-scale turbulent-laminar states in transitional pipe flow. *Proc. Natl Acad. Sci. USA* **107** (18), 8091–8096.

MULLIN, T. 2011 Experimental studies on transition to turbulence in a pipe. *Annu. Rev. Fluid Mech.* **43**, 1–24.

NISHI, M., ÜNSAL, B., DURST, F. & BISWAS, G. 2008 Laminar-to-turbulent transition of pipe flows through puffs and slugs. *J. Fluid Mech.* **614**, 425–446.

NOORANI, A., EL KHOURY, G. K. & SCHLATTER, P. 2013 Evolution of turbulence characteristics from straight to curved pipes. *Intl J. Heat Fluid Flow* **41**, 16–26.

NOORANI, A. & SCHLATTER, P. 2015 Evidence of sublaminar drag naturally occurring in a curved pipe. *Phys. Fluids* **27** (3), 035105.

PRINGLE, C. C. T. & KERSWELL, R. R. 2010 Using nonlinear transient growth to construct the minimal seed for shear flow turbulence. *Phys. Rev. Lett.* **105**, 154502.

REYNOLDS, O. 1883 An experimental investigation of the circumstances which determine whether the motion of water shall he direct or sinuous, and of the law of resistance in parallel channels. *Phil. Trans. R. Soc. Lond.* **174**, 935–982.

SCHANEN, M., MARIN, O., ZHANG, H. & ANITESCU, M. 2016 Asynchronous two-level checkpointing scheme for large-scale adjoints in the spectral-element solver Nek5000. *Procedia Comput. Sci.* **80**, 1147–1158.

SHIH, H.-Y., HSIEH, T.-L. & GOLDENFELD, N. 2015 Ecological collapse and the emergence of travelling waves at the onset of shear turbulence. *Nat. Phys.* **12**, 245–248.

SHIMIZU, M., MANNEVILLE, P., DUGUET, Y. & KAWAHARA, G. 2014 Splitting of a turbulent puff in pipe flow. *Fluid Dyn. Res.* **46** (6), 061403.

SONG, B., BARKLEY, D., HOF, B. & AVILA, M. 2017 Speed and structure of turbulent fronts in pipe flow. *J. Fluid Mech.* **813**, 1045–1059.

SREENIVASAN, K. R. & STRYKOWSKI, P. J. 1983 Stabilization effects in flow through helically coiled pipes. *Exp. Fluids* **1** (1), 31–36.

WEBSTER, D. R. & HUMPHREY, J. A. C. 1993 Experimental observations of flow instability in a helical coil (data bank contribution). *Trans. ASME J. Fluids Engng* **115** (3), 436–443.

WEBSTER, D. R. & HUMPHREY, J. A. C. 1997 Traveling wave instability in helical coil flow. *Phys. Fluids* **9** (2), 407–418.

WHITE, C. M. 1929 Streamline flow through curved pipes. *Proc. R. Soc. Lond.* A **123** (792), 645–663.

WYGNANSKI, I. J. & CHAMPAGNE, F. H. 1973 On transition in a pipe. Part 1. The origin of puffs and slugs and the flow in a turbulent slug. *J. Fluid Mech.* **59** (2), 281–335.

WYGNANSKI, I. J., SOKOLOV, M. & FRIEDMAN, D. 1975 On transition in a pipe. Part 2. The equilibrium puff. *J. Fluid Mech.* **69** (2), 283–304.